# Phase stability and structure of spinel-based transition aluminas

C. Wolverton and K. C. Hass
*Ford Research Laboratory, MD3028/SRL, Dearborn, Michigan 48121-2053*
(Received 26 June 2000; published 11 December 2000)

Using first-principles total energy calculations, we have investigated the structure and phase stability of spinel-based transition aluminas ($\gamma, \delta, \eta$), both in the presence and absence of hydrogen. The spinel-based structures (formed from dehydration of aluminum hydroxides) necessarily must have vacant cation positions to preserve the $Al_2O_3$ stoichiometry, and may have residual hydrogen cations in the structure as well. In the absence of hydrogen, we find the following: (i) Vacancies in octahedral sites are energetically preferred (or, Al cations prefer tetrahedral positions). (ii) There is a strong Al-vacancy ordering tendency, with widely separated vacancies being lower in energy than near-neighboring vacancies. Upon incorporation of hydrogen into the structure: (iii) The strong cation-vacancy ordering tendency vanishes, and ''clusters'' of near-neighbor vacancies are slightly energetically preferred. (iv) The hydrogen spinel ($HAl_5O_8$) proposed in the literature as a structural candidate for $\gamma$-alumina, is thermodynamically unstable with respect to decomposition into the anhydrous defect spinel plus boehmite ($\gamma$-AlOOH). (v) The temperature range for transforming boehmite into $\gamma$-$Al_2O_3$ is calculated from first-principles energetics plus measured thermochemical data of $H_2O$, and is in excellent agreement with the observed transformation temperatures. Finally, we comment on the possible implications of this work on the porous microstructure of the transition aluminas.

DOI: 10.1103/PhysRevB.63.024102 PACS number(s): 61.66.Fn, 64.70.Kb, 81.30.Hd, 71.15.Dx

## I. INTRODUCTION

Aluminum oxide or alumina, $Al_2O_3$, exhibits a remarkable series of structural polymorphs. In addition to the stable oxide $\alpha$-$Al_2O_3$ (corundum), there exist a large variety of metastable forms of alumina.[1–3] Among these metastable variants are a series of transition aluminas, which form as aluminum hydroxides and oxyhydroxides are dehydrated. The sequence of aluminas produced by dehydration of boehmite ($\gamma$-AlOOH) is particularly interesting:[4]

$$\text{boehmite} \rightarrow \gamma \rightarrow \delta \rightarrow \theta \rightarrow \alpha. \quad (1)$$

$\gamma$-$Al_2O_3$ produced from boehmite is an extremely important technological material:[5–8] $\gamma$ (and to some extent, $\delta$ and $\theta$) is used as high surface-area support material for automotive and other types of catalysts; it is used as a catalyst itself in petroleum refining; and it can be formed as an electrolytic oxide layer on aluminum. Thus, an enormous amount of effort has gone into understanding the nature of these transformations and the crystal structures of the various phases (see, e.g., Refs. 1–3,9–42).

However, there are still many open questions regarding the formation, structure, and even stoichiometry of $\gamma$. The transition aluminas $\gamma$, $\delta$, and $\theta$ all possess a face-centered-cubic (fcc) array of oxygen anions with the aluminum cations occupying a portion of the available octahedral and tetrahedral interstices. [This distinguishes these metastable phases from those based on a hexagonal close-packed (hcp) array of oxygen anions, such as $\kappa$, $\chi$, and the stable form $\alpha$.[1]] Although the structure of $\theta$ is generally accepted to be that of $\beta$-$Ga_2O_3$,[9,43–47] the crystal structures of $\gamma$ and $\delta$ have been hotly debated for the last half-century. The $\gamma$ and $\delta$ phases (along with another transition alumina, $\eta$) are generally believed to be based on a spinel structure. The cubic spinel structure (space group $Fd\bar{3}m$), usually denoted $AB_2O_4$, possesses an fcc sublattice of oxygen ions, with $A$ and $B$ cations occupying the tetrahedral ($T_d$) and octahedral ($O_h$) interstices, with Wyckoff positions $8a$ and $16d$, respectively [Fig. 1(a)]. There are also unoccupied tetrahedral ($8b$ and $48f$) and octahedral ($16c$) interstices of the oxygen sublattice [Fig. 1(b)]. (We refer the interested reader to Ref. 48 for a thorough description of the spinel structure, and the occupied/unoccupied Wyckoff positions.) The total cation-:anion ratio for the spinel structures is 3:4, and thus creating an $Al_2O_3$ phase (with cation:anion = 2:3) in the spinel struc-

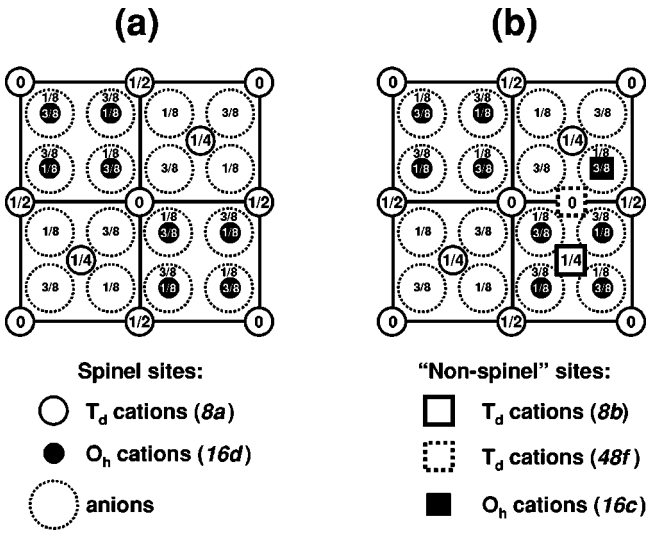


FIG. 1. Illustration of atomic sites in the spinel structure, shown as a (001) projection. The $z$ coordinate out of the page for each atom in an ideal spinel is shown in units of the lattice parameter. (a) The sites fully occupied in a normal spinel: the cubic-close-packed anion sublattice, and the $T_d$ ($8a$) and $O_h$ ($16d$) cation sites. (b) Representative ''nonspinel'' interstices: $T_d$ ($8b$ and $48f$) sites and $O_h$ ($16c$) sites.

 

ture necessitates creating vacancy defects on the cation sublattice. Thus, the spinel-based alumina structures are often referred to as defect spinels. Additionally, since the spinel structure contains two symmetrically distinct cation sites, the question naturally arises whether the vacant sites should be on the $T_d$ or $O_h$ sites. In an ideal spinel, 33.3% of the cations are tetrahedral and 66.7% are octahedral. In an $Al_2O_3$-based defect spinel, the percentages of $T_d$ and $O_h$ cations can theoretically range from 25% $T_d$ and 75% $O_h$ (if all vacancies are on $T_d$ sites) to 37.5% $T_d$ and 62.5% $O_h$ (if all vacancies are on $O_h$ sites).[49]

Although $\gamma$, $\delta$, and $\eta$ are all believed to be spinel-based, these phases are generally distinguished from one another as follows: $\eta$ is a dehydration product of $\alpha$-$Al(OH)_3$, *bayerite*, whereas $\gamma$ and $\delta$ are dehydration products of boehmite. $\delta$-$Al_2O_3$ is formed subsequent to $\gamma$ in sequence (1) and may be distinguished from $\gamma$ in diffraction experiments by superstructure reflections which appear in the $\delta$ phase, but not in $\gamma$. The precise structure of $\delta$ is not known, although it has been described[10,11] as a superlattice of the spinel structure with ordered vacancies. Levin and Brandon[1] have argued that $\delta$ (and $\theta$) are formed from the $\gamma$ phase by cation ordering on the interstices of the fcc oxygen sublattice, which is itself relatively undisturbed during the transformation.

For each of the phases ($\gamma$, $\delta$, and $\eta$), one would like to know the arrangement of cations (or the arrangement of vacancies) on the spinel sites. A wide variety of experimental methods has been used to try to ascertain this vacancy site preference; however, no definitive consensus has emerged. Many studies of the spinel-based aluminas have demonstrated a preference for vacancies on *octahedral* sites: For the $\gamma$ and $\eta$ phases, x-ray diffraction (XRD),[12–15] nuclear magnetic resonance (NMR),[16] electron microscopy (TEM and HRTEM) and selected-area electron diffraction[17,18] results have all been interpreted as evidence that vacancies primarily reside on $O_h$ positions. At least one of these papers[13] noted that the diffraction intensities obtained from various aluminas depends strongly on the preparation conditions. Recent HREM studies[17,18] have found an *ordering* of $O_h$ vacancies on (110) planes in $\gamma$ and $\delta$. Repelin and Husson[19] used XRD and electron diffraction to deduce a structural model of $\delta$ which contains 37.5% $T_d$ cations, consistent with exclusively $O_h$ vacancies in a defect spinel model. Using XRD, Ushakov *et al.* found $\sim$39–43 % $T_d$ cations in $\gamma$, an even larger tetrahedral occupation than can be accommodated within a defect-spinel framework. Other authors[14,20] have found a general migration of Al cations from $O_h$ to $T_d$ positions (or, a vacancy migration from $T_d$ to $O_h$ positions) as samples were annealed at increasingly higher temperatures. These studies suggest a thermodynamic preference for Al in $T_d$ positions ($O_h$ vacancies).

Other studies support the opposite conclusion, namely that vacancies tend to reside on *tetrahedral* positions: Some electron diffraction[21,22] and XRD (Ref. 23) data, for example, suggest a preference for $T_d$ vacancies. Several NMR studies[24–26] also support this conclusion for $\gamma$, although one of these studies[24] found a preference for $O_h$ vacancies in $\eta$; another of these studies[25] found that $\eta$ contains a random distribution of $T_d$ and $O_h$ vacancies.

To complicate the situation further, many authors have also suggested that $\gamma$, $\delta$, and $\eta$ contain significant portions of cations occupying sites which are vacant in the ideal spinel structure [e.g., 8*b*, 16*c*, 48*f*, and 32*e*, which we refer to as *''nonspinel'' sites*—see Fig. 1(b)]. Zhou and Snyder[9] performed neutron diffraction refinements of $\gamma$ and $\eta$, and found significant quantities of nonspinel site occupations: For $\gamma$, the refinements indicated not only occupation of the spinel 16*d* sites and 8*a* sites, but a significant fraction of atoms in 32*e* sites, which are close in position to the $O_h$ 16*c* sites. For $\eta$, these authors found occupation of 16*d* sites, no atoms in 8*a* sites, and significant occupations of the nonspinel 48*f* sites and 32*e* sites. The powder XRD data of Shirasuka *et al.*[15] suggest a significant occupation of nonspinel sites (48*f* and 16*c*) for $\eta$. Ushakov *et al.*[27] demonstrated that measured XRD patterns cannot be indexed with occupation of only spinel sites. The HRTEM results of Ernst *et al.*[28] suggest that $\eta$ contains $O_h$ cations in both 16*c* and 16*d* positions and $T_d$ cations in both 8*a* and 48*f* positions. Further, since one of the lattice parameters of $\delta$ is typically reported as a noninteger multiple (3/2) of the lattice parameter of $\gamma$, symmetry considerations alone suggest[1] that the $\gamma \rightarrow \delta$ transformation cannot proceed via a simple, direct ordering of $\gamma$, and hence some filling of both spinel and nonspinel sites must occur in the $\delta$ phase.

Adding another layer of complexity to this problem is the uncertain role of hydrogen: The transition aluminas are often characterized by high surface areas, and hydroxyl groups are well known to be ubiquitous on the internal and external surfaces (see, e.g., Refs. 29–31,50). In addition, there are several reports of H in the *bulk* of $\gamma$-$Al_2O_3$:[14,27,32–34] In analogy with the lithium spinel, $LiAl_5O_8$, de Boer and Houben[32] suggested the idea of the hydrogen spinel $HAl_5O_8$ as a hydrogenated form of $\gamma$-$Al_2O_3$. Ushakov *et al.*[27] could only account for measured XRD patterns of $\gamma$ with residual hydrogen (and nonspinel cation occupation) in the structure. Soled[29] considered the replacement of $O^{2-}$ ions in the structure with twice as many $OH^-$ ions (coming from surface hydroxyl groups), and demonstrated how varying amounts of hydrogen could appear in the chemical formula for $\gamma$ during the dehydration process. Tsyganenko *et al.*[33] found peaks in IR spectra which they attributed to vibrations of O-H groups not on the surface, but in the bulk. These authors also supported the ''protospinel'' ($HAl_5O_8$) hypothesis of de Boer and Houben. Using XRD and NMR, Wang *et al.*[14] found more cation defects than could be explained with a simple defect spinel. They attributed these extra cation defects to OH groups in the bulk, and observed that these groups were driven out of bulk with increasing annealing temperature. However, Zhou and Snyder[9] found only small amounts of hydrogen in $\gamma$, $\eta$, and $\theta$, and thus specifically ruled out the possibility of the hydrogen spinel as a structural candidate for the spinel-based phases.

Motivated in part by the wealth of experimental effort and lack of consensus, many theoretical efforts have also been aimed at elucidating the structure of spinel-based aluminas.

The results are equally confusing. Several authors have used empirical pair potentials to study the structure and energetics of $\gamma$-$Al_2O_3$. Mo *et al.*[35] found a large energetic preference for $O_h$ vacancies, in nonstoichiometric $Al_{21}O_{32}$ cells, considered as an approximation to $Al_2O_3$. Using a different pair potential form and molecular dynamics simulations, Alvarez *et al.*[36] found a preference for $T_d$ vacancies (Al atoms migrated from $T_d$ to $O_h$ positions during the simulation). Streitz and Mintmire[37] used more physically motivated empirical potentials than in the previous studies, and found an energetic preference for $O_h$ vacancies, with an energy scale much smaller than that found by Mo *et al*. Two studies of the structure of $\gamma$ have been performed using nonempirical, first-principles calculations. Lee *et al.*[26] used the pseudopotential density functional theory (DFT) code, CASTEP, in conjunction with Monte Carlo simulations, and found a disordered structure with 70% $O_h$ cations (which corresponds to a slight preference for $T_d$ vacancies in spinel). This study employed 20-atom cells with an unrelaxed anion sublattice; it was not limited to purely spinel-based configurations, but rather considered the more general problem of the lowest energy states of the cations in the interstices of an fcc oxygen sublattice. (We demonstrate below that the lowest energy fcc-based configuration should actually correspond to $\theta$-$Al_2O_3$, which has only 50% $O_h$ cations.) In a recent study, Sohlberg *et al.*[34] also used CASTEP to examine the role of hydrogen in aluminas. They found the hydrogen spinel to be far lower in energy than the anhydrous defect spinels (plus $H_2O$), and thus an inherent thermodynamic preference for hydrogen in the bulk of $\gamma$-alumina. If correct, this result would support the hydrogen spinel model of $\gamma$-alumina proposed by de Boer and Houben.[32] However, there is an unusually large error of 20% relative to experiment in Ref. 34 for the calculated volume of corundum, $\alpha$-$Al_2O_3$, which raises doubts about the accuracy of the calculations. CASTEP was also the method of choice in two first-principles studies[38,39] of the non-spinel-based $\theta$ phase of $Al_2O_3$. Recently, in a remarkable use of first-principles DFT, Yourdshahyan *et al.*[51] elucidated the structure of the hexagonal transition phase, $\kappa$-$Al_2O_3$, for which the crystal structure was previously unknown, and verified their prediction against measured XRD patterns. That work inspires confidence that accurate first-principles calculations can be an effective tool for resolving structural issues in complex aluminas.

The time is thus ripe to reexamine the conflicting theoretical and experimental claims concerning the structure of spinel-based transition aluminas within a comprehensive, state-of-the-art, first-principles analysis. Given the large error in volume of $\alpha$-$Al_2O_3$ in the CASTEP calculations pointed out by Sohlberg *et al.*,[34] it is clear that any analysis of this type must include a critical and detailed assessment of the accuracy of the computational methods employed. In this paper, we investigate (a) the site preference (both spinel and non-spinel) of cations and vacancies in $\gamma$, $\delta$, and $\eta$ alumina, (b) the ordering of the vacancies, and (c) the effect of hydrogen on phase stability, all from a critically assessed DFT total energy approach. The existence of multiple distinct, spinel-based phases of alumina ($\gamma, \delta, \eta$) demonstrates that simple energy-lowering mechanisms cannot be responsible for the structures of all three phases. Thus, any study of those materials should consider not only the lowest-energy spinel-based state, but all likely configurations of cations and vacancies in the structure. Finally, it is important to note that although the spinel-based $\gamma$, $\delta$, and $\eta$ aluminas are highly porous materials with high surface areas, the present work is a study of ideal, nonporous *bulk* properties of these transition aluminas. Surface properties are not considered. The understanding of bulk properties is a necessary step towards understanding the surface properties, and it is anticipated that physical effects which control cation ordering and site preference in the bulk should help us to understand and create realistic surface models.

## II. METHODOLOGY

For the majority of the calculations to be described below, we have used the plane wave pseudopotential method, as implemented in the Vienna *ab initio* simulation package (VASP).[52] However, to test the accuracy and transferability of these pseudopotential results, we have critically compared many results computed with VASP with the more-accurate all-electron full-potential linearized augmented plane wave (FLAPW) method, using the code of Wei and Krakauer.[53] As we demonstrate below, VASP is extremely accurate with respect to FLAPW for a wide range of different structures, but the pseudopotential calculations are much more efficient than FLAPW and thus allow us to easily treat unit cell sizes which would be quite cumbersome to study with FLAPW.

In the FLAPW calculations, we used the local density approximation (LDA) with the exchange-correlation functional of Ceperley and Alder as parametrized by Perdew and Zunger.[54,55] FLAPW sphere radii were chosen to be 1.8, 1.3, and 0.5 a.u. for Al, O, and H, respectively. The valence electrons were treated semirelativistically, and the core electrons were treated fully relativistically, with no ''frozen core'' approximation. A well converged basis set was used, corresponding to an energy cutoff of 347 eV. Brillouin-zone integrations were performed using Monkhorst-Pack **k**-point meshes. All structures were fully relaxed with respect to volume as well as all cell-internal and -external coordinates. Convergence tests of the energy differences (with respect to basis function cutoff, **k**-point sampling, and muffin-tin radii) indicate that the total energy differences were converged to within $\sim 0.01$–$0.02$ eV/formula unit.

For the VASP calculations, ultrasoft pseudopotentials were used.[56,57] Since we are studying systems with tetrahedral Al-O bonds (which can be as small as 1.7 Å), it is important to verify that the core cutoff for the Al pseudopotential is sufficiently small to avoid significant core overlap. Partial core corrections[58] were included in the calculations. Calculations were performed both for the LDA, with the exchange-correlation functional of Ceperley and Alder,[54,55] and for the generalized gradient approximation (GGA) of Perdew and Wang.[59] All structures were fully relaxed with respect to volume as well as all cell-internal and -external coordinates. Extensive tests indicated that 495 eV was a suf-

TABLE I. Comparison of calculated (FLAPW and VASP) and experimental lattice constants (in Å) and structural parameters for $\alpha$-$Al_2O_3$, given in terms of the primitive rhombohedral unit cell. $a$ and $\alpha$ are the lattice constant and rhombohedral angle, whereas $w$ and $u$ are the cell-internal parameters for Al and O atoms, respectively, and $V$ is the unit cell volume (in Å$^3$).

| Quantity | FLAPW (LDA) | VASP (LDA) | VASP (GGA) | Expt. (Ref. 80) |
|---|---|---|---|---|
| $a$ | 5.071 | 5.080 | 5.161 | 5.128 |
| $\alpha$ | 55.45 | 55.26 | 55.27 | 55.28 |
| $w$ (Al) | 0.352 | 0.352 | 0.352 | 0.352 |
| $u$ (O) | 0.556 | 0.556 | 0.556 | 0.556 |
| $V$ | 84.8 | 82.5 | 86.5 | 84.8 |

ficient cutoff to achieve highly accurate energy differences, and convergence tests of **k**-point sampling indicated that total energy differences were converged to within $\sim$0.01 eV/formula unit.

## III. ASSESSING THE ACCURACY OF THE PRESENT CALCULATIONS

Before performing a study of the spinel-based transition aluminas, it is prudent to verify the accuracy of the calculations for some other (non-spinel-based) aluminas for which the structures are known. The accuracy can be assessed by comparing the calculations to experiment for structural parameters of the phases as well as thermochemical data for heats of reactions between the various phases. Additionally, one should perform tests of the pseudopotentials versus all-electron calculations to verify the accuracy and transferability of the pseudopotential results. Toward this end, we have performed calculations for four well-characterized phases of alumina and two aluminum hydroxides: the stable $\alpha$ phase, $\theta$-$Al_2O_3$ (isomorphic with $\beta$-$Ga_2O_3$),[9,43–47] $\kappa$-$Al_2O_3$ (whose structure has recently been elucidated by first-principles calculations[51]), a hypothetical compound of $Al_2O_3$ in the bixbyite structure, $\gamma$-AlOOH (boehmite), and $\gamma$-$Al(OH)_3$ (gibbsite). We also compare our results with previous theoretical results in the literature in order to assess the accuracy of the current and previous calculations.

Table I lists the calculated and observed lattice constants and cell-internal positions for $\alpha$-$Al_2O_3$. Calculated results are given for the FLAPW method within the LDA, and for VASP within both the LDA and GGA. The calculated lattice constants show a level of agreement with experiment typical of solid-state DFT calculations: the LDA calculations underestimate the lattice constant by $\sim$1% relative to the experimentally observed value, whereas the GGA calculations overestimate the lattice constants by $\lesssim$1%. We also note that the cell-internal positions agree precisely (to three digits) with experimental refinements. Previous first-principles calculations of $\alpha$-$Al_2O_3$ using a variety of techniques (summarized in Ref. 60) have similar agreement with experiment for structural properties of $\alpha$-$Al_2O_3$. The results in Table I further demonstrate the accuracy of the VASP calculations: the LDA lattice constants and structural data obtained with VASP are in excellent agreement with the FLAPW results. This agreement of the present (and previous) calculations with experiment is particularly noteworthy in light of the $\sim$20% underestimation of the GGA-calculated volume of $\alpha$-$Al_2O_3$ reported in a recent first-principles study[34] of the role of hydrogen in $\gamma$-$Al_2O_3$. Such a large error between calculated and experimental structural properties is certainly not to be expected from state-of-the-art DFT calculations.

Table II shows a similar comparison between the calculated and observed lattice constants and cell-internal positions for $\theta$-$Al_2O_3$ in the $\beta$-$Ga_2O_3$ structure. Calculated results are shown for the FLAPW method within the LDA and

TABLE II. Comparison of calculated (FLAPW and VASP) and experimental structural properties of $\theta$-$Al_2O_3$. Lattice constants $(a,b,c)$ are in Å, $\beta$ is the monoclinic angle, $V$ is the unit cell volume (in Å$^3$), and $(x,z)_i$ are the cell-internal positions for atom $i$.

| Property | FLAPW (LDA) | VASP (LDA) | VASP (GGA) | Expt. (Ref. 9) | Expt. (Ref. 43) | Expt. (Ref. 47) |
|---|---|---|---|---|---|---|
| $a$ | 11.77 | 11.66 | 11.87 | 11.85 | 11.81 | 11.80 |
| $b$ | 2.910 | 2.881 | 2.929 | 2.904 | 2.906 | 2.910 |
| $c$ | 5.591 | 5.568 | 5.657 | 5.622 | 5.625 | 5.621 |
| $\beta$ | 104.1 | 104.1 | 104.0 | 103.8 | 104.1 | 103.8 |
| $V$ | 92.9 | 90.7 | 95.4 | 93.9 | 93.6 | 93.7 |
| $(x,z)_{Al1}$ | (0.909,0.204) | (0.909,0.204) | (0.910,0.204) | (0.917,0.207) | (0.916,0.207) | (0.899,0.206) |
| $(x,z)_{Al2}$ | (0.658,0.317) | (0.658,0.317) | (0.658,0.317) | (0.660,0.316) | (0.660,0.317) | (0.648,0.313) |
| $(x,z)_{O1}$ | (0.162,0.109) | (0.162,0.109) | (0.159,0.109) | (0.161,0.098) | (0.161,0.107) | (0.163,0.123) |
| $(x,z)_{O2}$ | (0.495,0.257) | (0.495,0.257) | (0.495,0.257) | (0.495,0.253) | (0.498,0.260) | (0.489,0.261) |
| $(x,z)_{O3}$ | (0.827,0.435) | (0.827,0.435) | (0.826,0.432) | (0.827,0.427) | (0.833,0.440) | (0.830,0.439) |

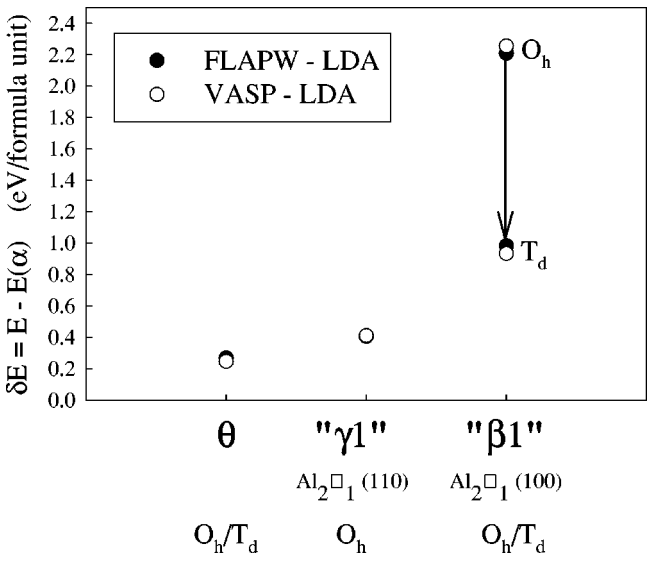


FIG. 2. Comparison of $Al_2O_3$ energy differences calculated from FLAPW and VASP. Shown are the energies of three structures, relative to $\alpha$-$Al_2O_3$: $\theta$, ''$\gamma 1$,'' and ''$\beta 1$.'' The latter two are hypothetical structures formed from a tripled rocksalt supercell ($Al_3O_3$) by removing one Al atom.

for VASP within both the LDA and GGA. Just as in the case of $\alpha$, the calculated lattice constants and cell-internal positions for $\theta$-$Al_2O_3$ show an excellent agreement with experiment: the LDA calculations underestimate the lattice constant by $\sim$1% relative to the experimentally observed values, whereas the GGA calculations overestimate the lattice constants by $\lesssim$1%. Again, the cell-internal positions agree well with experimental refinements (errors are in the third decimal place, and often are no larger than the differences between the experimental refinements). And, the LDA lattice constants and structural data obtained with VASP are in excellent agreement with the FLAPW results. In fact, the VASP-(LDA) relaxed geometry was used as the starting geometry for the FLAPW calculations, and it was found (by examining the FLAPW forces in this geometry) that the cell-internal degrees of freedom were already optimized. Also, neither Table I nor Table II show a clear ''winner'' in terms of physical accuracy between LDA and GGA in describing $Al_2O_3$.

From Tables I and II, we have demonstrated the accuracy of VASP relative to FLAPW for *structural* properties of alumina. Figure 2 shows the *energetics* of several fully relaxed $Al_2O_3$ cells as calculated from VASP and FLAPW. Shown are the energies (relative to $\alpha$) of the $\theta$ structure, as well as ''$\gamma 1$'' and ''$\beta 1$,'' two hypothetical 5-atom cells formed from a tripled rocksalt supercell ($Al_3O_3$) by removing one Al atom. In rocksalt, all the cations are octahedrally coordinated. For the ''$\beta 1$'' structure, it is possible to move one of the cations into a tetrahedral site, and thus we have calculated the energetics of this structure before (labeled ''$O_h$'') and after (labeled ''$T_d$'') this move. Figure 2 demonstrates that the VASP energetics are also extremely accurate relative to FLAPW for a nontrivial range of different geometries, including both $O_h$ and $T_d$ coordinated aluminum atoms.

Table III shows comparisons between first-principles calculated and experimentally measured structural data for the aluminum oxyhydroxide, $\gamma$-AlOOH (boehmite). The structure of boehmite was taken from the neutron diffraction refinements of Corbato *et al.*[61] These authors suggested a centered-orthorhombic $Cmcm$ space group with 8 atoms in the primitive cell, and hydrogen occupying 50% of the $8f$ positions. Some of the $8f$ positions are quite close together ($<$1 Å), and so we chose hydrogen occupation of the $8f$ sites so as to avoid these near-neighboring positions. This choice resulted in zigzag O-H$\cdots$O-H$\cdots$O-H$\cdots$ chains as described by Wickersheim and Korpi.[62] Additionally, since there has been some discussion in the literature about O-H bond lengths, H-O-H bond angles, and the correct space group for this structure (see the discussion in Ref. 61), we performed a calculation starting with small random displacements of atoms relative to the Corbato *et al.* structure, such that the initial structure contained only $P1$ symmetry. All atoms relaxed back to the Corbato *et al.* structure with the following geometry: O-H bond length of 1.01 Å, and a O-H$\cdots$O bond angle of $\sim$180°. Both of these calculated geometrical features are in excellent agreement with neutron diffraction data,[61] as are the calculated lattice constants and cell-internal parameters of boehmite. As expected, the GGA exchange-correlation functional is more accurate for the oxyhydroxide than the LDA, due to the more accurate description of hydrogen bonding within the GGA.[63] Additionally, the comparison of VASP and FLAPW within the LDA dem-

TABLE III. Comparison of calculated (FLAPW and VASP) and experimental structural properties of boehmite ($\gamma$-AlOOH). Lattice constants are in Å, $V$ is the unit cell volume (in Å$^3$), and the $u$'s are the cell-internal parameters.

| Property | FLAPW (LDA) | VASP (LDA) | VASP (GGA) | Expt. (Ref. 61) |
|---|---|---|---|---|
| $a$ | 2.844 | 2.834 | 2.887 | 2.868 |
| $b$ | 11.82 | 11.60 | 12.09 | 12.234 |
| $c$ | 3.681 | 3.668 | 3.722 | 3.692 |
| $V$ | 123.8 | 120.6 | 130.0 | 129.5 |
| $u_{\mathrm{Al}}$ | -0.321 | -0.321 | -0.319 | -0.318 |
| $u_{\mathrm{O}_1}$ | 0.292 | 0.292 | 0.290 | 0.290 |
| $u_{\mathrm{O}_2}$ | 0.074 | 0.074 | 0.078 | 0.078 |
| $u_{\mathrm{H}}$ | (0.013,0.047) | (0.013,0.047) | (0.019,0.061) | (0.024,0.069) |

TABLE IV. Comparison of calculated (VASP-GGA) and experimental structural properties of gibbsite, $Al(OH)_3$. Lattice constants are in Å, $\beta$ is the monoclinic angle, $V$ is the unit cell volume (in Å$^3$), and $(x,y,z)_i$ are the cell-internal positions for atom $i$.

| Property | VASP (GGA) | Expt. (Ref. 64) |
|---|---|---|
| $a$ | 8.727 | 8.684 |
| $b$ | 5.091 | 5.078 |
| $c$ | 9.645 | 9.736 |
| $\beta$ | 92.65 | 94.54 |
| $V$ | 428.1 | 428.0 |
| $(x,y,z)_{Al1}$ | (0.167, 0.536, -0.002) | (0.168, 0.530, -0.002) |
| $(x,y,z)_{Al2}$ | (0.335, 0.027, -0.002) | (0.334, 0.024, -0.002) |
| $(x,y,z)_{O1}$ | (0.181, 0.222, -0.112) | (0.178, 0.218, -0.112) |
| $(x,y,z)_{O2}$ | (0.672, 0.650, -0.104) | (0.669, 0.656, -0.102) |
| $(x,y,z)_{O3}$ | (0.503, 0.132, -0.106) | (0.498, 0.132, -0.104) |
| $(x,y,z)_{O4}$ | (-0.018, 0.634, -0.108) | (-0.020, 0.629, -0.107) |
| $(x,y,z)_{O5}$ | (0.299, 0.723, -0.106) | (0.297, 0.718, -0.105) |
| $(x,y,z)_{O6}$ | (0.826, 0.142, -0.105) | (0.819, 0.149, -0.102) |
| $(x,y,z)_{H1}$ | (0.079, 0.142, -0.123) | (0.101, 0.152, -0.124) |
| $(x,y,z)_{H2}$ | (0.576, 0.549, -0.102) | (0.595, 0.573, -0.098) |
| $(x,y,z)_{H3}$ | (0.500, 0.114, -0.208) | (0.503, 0.137, -0.190) |
| $(x,y,z)_{H4}$ | (-0.050, 0.819, -0.112) | (-0.029, 0.801, -0.107) |
| $(x,y,z)_{H5}$ | (0.296, 0.724, -0.209) | (0.293, 0.724, -0.196) |
| $(x,y,z)_{H6}$ | (0.812, 0.158, -0.208) | (0.815, 0.160, -0.190) |

onstrates that the pseudopotential approach is nearly as accurate for aluminum oxyhydroxides as for pure aluminas.

Table IV shows the comparison between calculated (VASP-GGA) and experimental structural properties of gibbsite, $\gamma$-$Al(OH)_3$. The structure used for gibbsite is that of Saalfeld and Wedde,[64] a monoclinic phase with 56 atoms per cell. The calculated lattice constants are in reasonable agreement with experiment, particularly for such a complex, low-symmetry structure. The Al and O cell-internal positions also agree well with the XRD refinements of Saalfeld and Wedde, although there is a larger disparity in the H positions. Saalfeld and Wedde found O-H bond lengths in their refinements of 0.75–0.88 Å, whereas our calculated O-H bond lengths are 0.98–1.00 Å which are in better agreement with O-H bond lengths measured in many other compounds. Saalfeld and Wedde themselves point out that x-ray determinations yield shorter O-H distances than neutron diffraction. Thus, we assert that our calculated H positions are probably more accurate than the x-ray refined positions, and the disparity between calculated/measured H positions is due to the use of XRD in the work of Saalfeld and Wedde.[64] The calculated positions in Table IV can therefore serve as a prediction for any future neutron diffraction refinements of the $Al(OH)_3$ gibbsite structure.

The extensive comparisons of VASP vs FLAPW, LDA vs GGA, and calculation vs experiment in Tables I–IV instill confidence in the accuracy of our first-principles calculations to describe both geometric and energetic properties of aluminum oxides and hydroxides. The VASP (GGA) calculations in particular appear to provide both the accuracy and computational efficiency necessary to study properties of the various phases of alumina, both with and without hydrogen. As a further test of this approach, and in order to assess the accuracy of a number of previous calculations for non-spinel-based aluminas, we have also performed calculations for $\kappa$-$Al_2O_3$ (Ref. 51) and alumina in the bixbyite structure. Table V compares our results for the energetics of these structures and $\theta$-$Al_2O_3$ with previous calculations, where available. All calculations correctly predict all of the energy differences, $\delta E(\theta-\alpha)$, $\delta E(\text{bixbyite}-\alpha)$, and $\delta E(\kappa-\alpha)$, to be positive, which is consistent with $\alpha$ being the most stable of the four candidate structures. Our VASP results for the $\kappa-\alpha$ energy differences agree well with the results of Yourdshahyan *et al.*[51] obtained with the DACAPO code. All of the calculated $\kappa-\alpha$ energy differences are in the neighborhood of the experimental value. There are, however, signifi-

TABLE V. First-principles calculated $Al_2O_3$ energy differences (eV/formula unit): $\delta E(\theta-\alpha)$, $\delta E(\text{bixbyite}-\alpha)$, and $\delta E(\kappa-\alpha)$.

| | Method | $\delta E(\theta-\alpha)$ | $\delta E(\text{bixbyite}-\alpha)$ | $\delta E(\kappa-\alpha)$ |
|---|---|---|---|---|
| | Expt. (Ref. 65) | $<0.12$[a] | | 0.16 |
| Present Work | FLAPW (LDA) | 0.27 | | |
| Present Work | VASP (LDA) | 0.25 | 0.21 | 0.21 |
| Present Work | VASP (GGA) | 0.04 | 0.16 | 0.08 |
| Ref. 51 | Pseudopotential (LDA) | | | 0.15 |
| Ref. 51 | Pseudopotential (GGA) | | | 0.09 |
| Ref. 38 | Pseudopotential (LDA) | 0.57 | 0.73 | |
| Ref. 39 | FLAPW (LDA) | 0.66 | 0.72 | |
| Ref. 39 | FLMTO (LDA) | 0.70 | 0.56 | |
| Ref. 39 | Pseudopotential (LDA) | 0.38 | 0.97 | |
| Ref. 81 | LCAO | 0.44 | | |
| Ref. 82 | Hartree-Fock | 0.44 | | |

[a]Yokokawa and Kleppa (Ref.65) measured the enthalpy difference between $\delta$ and $\alpha$ as 0.12 eV/formula unit. Since $\delta$ transforms to $\theta$ before $\alpha$ (see, however, Ref. 4), we surmise that the enthalpy of $\theta$ must be below that of $\delta$, and thus the $\theta-\alpha$ enthalpy difference must be less than $\delta-\alpha$.

cant disparities between the present results and previous calculations of the $\theta-\alpha$ and bixbyite$-\alpha$ energy differences. Previous calculations[38,39,81,82] found much larger energy differences $\delta E(\theta-\alpha)$ and $\delta E$(bixbyite$-\alpha$) than in the present work. In the case of $\theta$-$Al_2O_3$, measurements put an upper bound on the transformation energy of $\delta E(\theta-\alpha) < 0.12$ eV/formula unit.[65] The present VASP (GGA) calculations fall below this upper bound ($\delta E = 0.04$ eV), whereas the present LDA results lie above ($\delta E = 0.25$ and 0.27 eV for FLAPW and VASP, respectively). This suggests that the GGA results are more accurate than the LDA even for anhydrous structures. All of the previous results[38,39,81,82] ($\delta E = 0.38$–$0.70$ eV) lie far above the experimental upper bound.

There exists an interesting correlation between oxygen sublattice stacking and cation site preference for the $\alpha$, $\kappa$, and $\theta$ structures: The oxygen sublattices for these three structures are all close packed, but while the $\alpha$ structure contains a hexagonal stacking ($ABAB$), the $\theta$ structure has an fcc stacking ($ABCABC$), with $\kappa$ being intermediate between the two ($ABAC$). The $\alpha$ structure has purely $O_h$ cations, whereas $\theta$ has 50% $O_h$ and 50% $T_d$. Again, the $\kappa$ structure is intermediate between these extremes, with 75% $O_h$ and 25% $T_d$ cations.[51] Thus, we note the increasing preference for $T_d$ cations as the oxygen sublattice planes change from hcp to fcc stackings. As we show below, this $T_d$ cation preference will carry over into the defect spinel configurations (fcc stacking) as well.

## IV. ANHYDROUS SPINEL-BASED STRUCTURES: $Al_2O_3$

To study the energetics of various defect spinel configurations, we begin by defining the spinel supercell used. One requires a supercell with an integer number of spinel primitive unit cells (the primitive unit cell of spinel contains 14 atoms), and an integer number of vacancies to obtain the $Al_2O_3$ stoichiometry. The smallest such supercell contains 40 atoms: 3 spinel units (42 atoms) with two cation vacancies, or $Al_{16}O_{24} = 8$ $Al_2O_3$ formula units. The spinel structure has fcc cell vectors, and so the 40-atom spinel supercell will correspond to a tripled fcc cell. From lattice algebra techniques,[66] we immediately find that there are exactly three possible supercell shapes: orthorhombic, tetragonal, and rhombohedral, corresponding to stackings of fcc units along (110), (100), and (111), respectively. We chose the orthorhombic cell with (110) stacking, since it is the most ''compact'' (i.e., the longest supercell vector is smaller than in either the tetragonal or rhombohedral case), and hence should provide the best opportunity for widely spacing the periodically repeated vacancies in all three dimensions. (Some tests were also performed with the tetragonal-shaped supercell.) Within this orthorhombic supercell, the two vacancies can be placed in a variety of cation positions: Both can be placed on $O_h$ sites, both on $T_d$ sites, or one on each. Furthermore, the distance between the two vacancies can also be varied.

We have performed total energy calculations for nine such orthorhombic supercells, both within the LDA and the GGA. In all cases, the supercells were fully relaxed with respect to cell-internal and -external degrees of freedom, starting from the ''ideal'' spinel geometry (with perfect, undistorted octahedra and tetrahedra). The results of these total energy calculations are shown (relative to $\alpha$) in Fig. 3. Several interesting points result from these calculations.

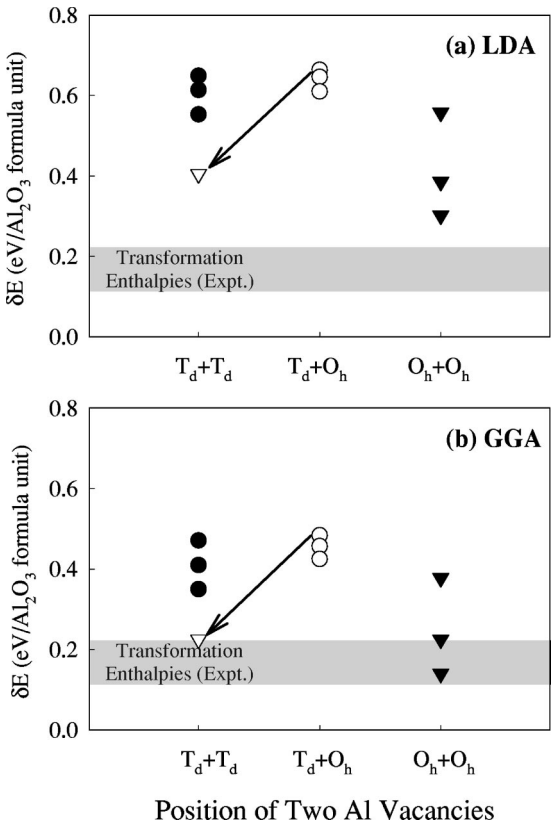


FIG. 3. LDA and GGA energetics of spinel-based $Al_2O_3$ supercells. Each of these points represents a 40-atom tripled spinel supercell with two vacant spinel cation positions. The gray band shows the range of measured enthalpies of transformation for the $\gamma$-$\alpha$ and $\delta$-$\alpha$ transitions. The inverted triangle represents a configuration which showed spontaneous relaxation of a cation into a ''nonspinel'' 16*c* site (see text for a description).

(1) *Energetic dependence on the cation configuration*. There is a strong energetic dependence on the cation/vacancy configuration. For LDA (GGA), the range between the lowest and highest energy defect spinel configuration is 0.35 (0.33) eV/formula unit. This energetic dependence on configuration should be contrasted with the energy difference between the lowest energy defect spinel and $\alpha$-$Al_2O_3$; for LDA (GGA), this energy difference is 0.30 (0.14) eV/formula unit. Thus, the configurational dependence of the energy is quite significant compared to the $\gamma$-$\alpha$ energy itself.

(2) *Vacancy site preference*. Vacancies on octahedral sites are energetically strongly preferred. Put another way, there is a strong tetrahedral site preference for Al cations. Although one might expect an octahedral site preference for Al, given the fact that the stable $\alpha$ phase possesses only $O_h$ coordinated cations, there is strong evidence for a tetrahedral site preference for Al in other alumina structures: Diffuse scattering measurements[67] of liquid $Al_2O_3$, for example, show a preponderance of fourfold coordinated Al. Recent DFT cal-

culations of ultrathin alumina films also suggest a preference for tetrahedral Al.[68] And finally, the calculated tetrahedral cation preference in the spinel-based structure is consistent with the stability of the $\theta$ phase, which has 50% tetrahedral cations (more than any of the defect spinel configurations), and an fcc stacking of oxygen atoms. The calculated energy of $\theta$ is lower than any of the defect spinel structures, and experimentally, $\theta$ is the ''end product''[4] in the transition aluminas before the transition to $\alpha$, which has an hcp oxygen sublattice: i.e., it is reasonable to assume that $\theta$ is the lowest energy fcc-based phase. This assertion is consistent with the conclusion of Zhou and Snyder that ''$\theta$-alumina should be considered as the ultimate rather than the intermediate structural form into which the transition aluminas could evolve on the way to corundum.''[9] Thus, the transformation from boehmite (0% $T_d$ cations) to $\theta$ (50% $T_d$) via spinel-based $\gamma$ and $\delta$ (25–37.5 % $T_d$) involves both a gradual reduction in energy accompanied by a gradual progression of cations into $T_d$ sites. Our calculated energetic preference for cations to occupy $T_d$ sites in the spinel-based structures is consistent with this progression.

(3) *Vacancy ordering*. Energetically, vacancies tend to be widely separated. The lowest energy configurations in Fig. 3 correspond to vacancies which are widely separated, with the energy of nearest-neighboring vacancies being much higher. This preference for vacancy separation is true regardless of whether one has $T_d$ or $O_h$ vacancies. Both points (2) and (3) are corroborated by a simple point-charge electrostatic model.[69] Also, our lowest-energy spinel supercell corresponds to ordered $O_h$ vacancies along (110) planes, in agreement with the recent observations of Wang *et al.*[17] and Kryukova *et al.*[18] on $\gamma$- and $\delta$-$Al_2O_3$.

(4) *Crystal structures of* $\delta$-$Al_2O_3$. Because the $\delta$ phase is considered to be derived from the $\gamma$ phase via cation ordering, it is likely that the lowest-energy ordered structures in Fig. 3 correspond more closely to $\delta$ than to $\gamma$. However, the analysis of Levin and Brandon[1] demonstrated that some nonspinel occupation is present in the $\delta$ phase, whereas the lowest-energy supercells considered in Fig. 3 contain only spinel-based cation occupation. Repelin and Husson[19] derived a crystal structure model for the $\delta$-$Al_2O_3$ phase based on XRD refinements. This model contains 37.5% $T_d$ cations, equal to that of the spinel supercells with purely $O_h$ vacancies, in agreement with our calculated energetic preference for $O_h$ vacancies. However, the fractional occupation of the $O_h$ sites given in Ref. 19 does not provide specific placement of the vacancies. We have performed first-principles calculations (VASP-GGA) of this 80-atom model of the $\delta$ phase, with two choices of the $O_h$ vacancies (not shown in Fig. 3). The resulting energies (relative to $\alpha$-$Al_2O_3$) are 0.35 and 0.45 eV/formula unit, which are above or near the high end of the spinel-based structures in Fig. 3 with $O_h$ vacancies (0.14, 0.22, and 0.38 eV/formula unit). Nevertheless, a more complete analysis of the energetically preferred vacancy configurations in this model could prove fruitful in finally identifying the crystal structure of $\delta$.

(5) *Comparison with experimental transformation enthalpies*. The LDA and GGA results are extremely similar, and all of the above qualitative results are true for either functional. However, there is a nearly constant shift between the LDA and GGA total energy differences relative to the $\alpha$ phase. To assess which is more accurate, we compare our $T=0$ calculated defect spinel energies (relative to $\alpha$) with measured thermochemical data of the enthalpies of transformation: $\Delta H(\delta-\alpha)$ and $\Delta H(\gamma-\alpha)$. Yokokawa and Kleppa[65] have measured these values calorimetrically and obtained 0.12 and 0.23 eV/formula unit, respectively. The experiments of Navrotsky *et al.*[40] yielded $\Delta H(\gamma-\alpha)=0.24$ eV/formula unit. By analyzing the effects of thermochemical data on surface area, McHale *et al.*[30] extrapolated the enthalpy of reaction to coarse-grained, or low-surface-area bulk materials and found $\Delta H(\gamma-\alpha)=0.14$ eV/formula unit. Thus, in Fig. 3, we have indicated a region between 0.12 and 0.24 eV/formula unit as ''experimental transformation enthalpies.'' The GGA clearly does a much better job of reproducing these measured enthalpies than does the LDA; several of the GGA supercell energies fall within the experimental region, whereas none of the LDA energies do. We have already shown in Table V that the GGA energetics for $\theta$ are also more consistent with measured enthalpies than corresponding LDA energetics. We conclude that the GGA gives a consistently superior (or, at least equally good) description of the structure and energetics of $Al_2O_3$ polymorphs. And, again, since we expect this superiority to be even more pronounced in the case of structures containing hydrogen (cf. Table III and Ref. 63) we adopt only GGA calculations in Secs. V and VI.

(6) *Cation occupation of nonspinel sites*. We have found two pieces of evidence that suggest a partial occupation of ''nonspinel'' sites by Al. In the spinel structure, only the 8*a* $T_d$ and 16*d* $O_h$ cation sites are occupied while other $T_d$ (8*b* and 48*f*) and $O_h$ (16*c*) sites are unoccupied [Fig. 1(b)]. 16*c* sites: In one of the defect spinel supercells considered, we have found a spontaneous (i.e., barrierless) relaxation of a $T_d$ (8*a*) Al into an $O_h$ (16*c*) ''nonspinel'' site.[70] The configuration initially had one $T_d$ and one $O_h$ vacancy. During the computational process of geometric relaxation of this structure, the system very nearly converges without the motion into the 16*c* site, but then begins to experience larger forces and subsequently relaxes further, with the 8*a* cation moving into the 16*c* position. The final state configuration effectively contains the same number of tetrahedral/octahedral cations as in supercells with two $T_d$ vacancies. Thus, in Fig. 3, we have included schematically the higher-energy ''nearly local minimum'' as a $T_d+O_h$ vacancy supercell, and indicate by an arrow the relaxation into a $T_d+T_d$ vacancy supercell with nonspinel occupation (shown by an inverted triangle). The latter structure with 16*c* occupation is significantly lower in energy than any of the other $T_d+T_d$ defect spinel supercells investigated. Thus, we conclude that $T_d$ vacancies (although not preferred as strongly as $O_h$ vacancies) are more likely to occur energetically when they are accompanied by 16*c* nonspinel occupation. In fact, other than two of the supercells with purely $O_h$ vacancies, this supercell with nonspinel occupation is the only cell with a calculated energy (GGA) within the range of experimental transformation enthalpies. This conclusion is interesting in light of the neutron refinement of $\gamma$ performed by Zhou and Snyder,[9] which yielded

43% $O_h$ in 16*d* sites and 32% $T_d$ in 8*a* sites, but a significant fraction of $O_h$ atoms in nonspinel 32*e* sites. These 32*e* sites were labeled as ''quasioctahedral'' since they are very close ($\sim 0.3$ Å) to the octahedral 16*c* sites. Zhou and Snyder concluded that the occupation of these nonspinel sites must be attributed to atoms which rearrange themselves at the surface of $\gamma$. However, we have demonstrated that some of the nonspinel occupation could be attributed to the spontaneous relaxation mechanism we have demonstrated, even for atoms in the bulk. 48*f* sites: We did not find any spontaneous occupation of the nonspinel $T_d$ sites (either 8*b* or 48*f*). However, both x-ray[15,27] and neutron[9] refinements of both $\gamma$ and $\eta$-$Al_2O_3$ did find significant occupation of these sites. To investigate further, we began with an ideal spinel supercell (42 atoms, with no vacancies), and moved one of the $T_d$ (8*a*) atoms into a 48*f* site. This movement placed it artificially close to two $O_h$ cations, which happened to be nearest-neighbor cations. Thus, we took these two $O_h$ cations as our cation vacancies for the 40-atom cell, and we examined the relaxed energetics before and after the $8a \rightarrow 48f$ motion of the $T_d$ atom. Before the movement, the supercell is simply one of our defect spinel supercells in Fig. 3. It has two nearest-neighbor $O_h$ vacancies, and due to the cation/vacancy ordering tendency, the energy of this structure is relatively high: 0.378 eV/formula unit above $\alpha$ (GGA). However, after moving the $T_d$ atom to the 48*f* position, the energy drops to 0.284 eV/formula unit. Thus, for a structure with neighboring $O_h$ vacancies, there is a significant energy lowering mechanism associated with occupation of the nonspinel 48*f* sites. This is a possible explanation for some of the 48*f* occupation found in the $\eta$-$Al_2O_3$ (which is often acknowledged to possess more $O_h$ vacancies than $\gamma$): In their neutron diffraction refinements of $\eta$, Zhou and Snyder found *no* $T_d$ atoms in 8*a* sites, but a large percentage (16%) of $T_d$ cations in 48*f* sites. Shirasuka *et al.*[15] found that $T_d$ cations in $\eta$ are divided roughly equally between the 8*a* and 48*f* sites. And, Ushakov and Moroz[27] found a significant percentage of nonspinel $T_d$ and $O_h$ occupation in both $\eta$ and $\gamma$. Again, since our predicted energy lowering by nonspinel occupation is in the bulk, all of the observed 48*f* occupation in $\eta$ need not necessarily be associated with surface cations, as had been concluded by Zhou and Snyder.[9,71] Finally, we should note that the observed structure of $\theta$-$Al_2O_3$ itself provides evidence for nonspinel occupation. Analysis of the atomic positions in $\theta$ shows that the cation sites can be mapped onto both spinel and nonspinel sites.

(7) *Comparison with experimental measurements of density*. We can also compare the calculated volumes of the spinel-based supercells to experimental estimates of the volume (or density) of $\gamma$-$Al_2O_3$. As we have seen in Tables I, II, III, and IV, the calculated equilibrium volumes for a given structure may differ from experiment by a few percent. However, the *difference* in volume between two structures is expected to be far more accurate than the absolute volume itself. For instance, the experimental difference in volume between the $\alpha$ and $\theta$ structures is $V(\alpha)-V(\theta)=\sim -4.4$ to $-4.6$ Å$^3$/formula unit, with the range given by the uncertainty in the volume of $\theta$-$Al_2O_3$ (see, e.g., the three experimental values in Table II). VASP (GGA) calculations of this volume difference yield $-4.4$ Å$^3$/formula unit. Thus, although the individual volumes are only accurate to within $\sim 1$ Å$^3$/formula unit, the volume differences are far more reliable. With this in mind, we show in Fig. 4 the calculated volumes of the spinel-based supercells relative to the $\theta$ structures: $\delta V = V(\gamma/\eta) - V(\theta)$. There is a clear correlation between vacancy site preference and atomic volume, with the $O_h$ vacancies yielding smaller volumes and the $T_d$ vacancies yielding larger ones. This correlation is likely due to the fact that $T_d$ positions are geometrically smaller than $O_h$ positions. Thus, the lattice can relax inwards around the larger space left behind by an $O_h$ vacancy, but less so for a $T_d$ vacancy. In fact, the spinel-based supercells with $O_h$ vacancies typically have volumes smaller than that of $\theta$-$Al_2O_3$, while the $T_d$-vacancy supercells have larger volumes than $\theta$. Thus, these calculated volumes should provide a clear and direct comparison with experimentally measured volume differences between $\gamma$ and $\theta$. The densities of $\gamma$- and $\eta$-$Al_2O_3$ quoted in the review of Levin and Brandon[1] have been determined from measured lattice constants (i.e., the density of the phase itself, not the porous microstructure) to be in the range 3.65–3.67 g/cm$^3$. Converting this range of densities to volumes per formula unit, and subtracting the range of measured volumes for $\theta$ given in Table II, we obtain the measured range $\delta V(\text{expt.}) = -0.9$ to $-0.4$ Å$^3$/formula unit, indicated in Fig. 4. It is clear that the calculated spinel supercells with $O_h$ vacancies are the only structures which are consistent with this range. This is yet another indication that the spinel-based aluminas contain $O_h$ vacancies. This result is particularly significant because it is purely structural and independent of any energetic argument. Because the lowest-energy spinel-based structure is probably more characteristic of $\delta$ than $\gamma$ or $\eta$, the actual atomic configurations in $\gamma$ and $\eta$ are probably not driven exclusively by an energy-

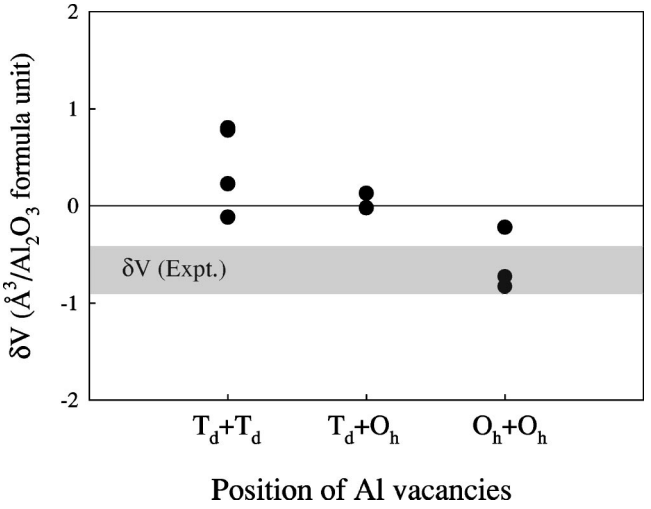


FIG. 4. Calculated (VASP-GGA) volume differences (Å$^3$/formula unit) between spinel-based $Al_2O_3$ supercells and $\theta$-$Al_2O_3$, $\delta V = V(\gamma/\eta) - V(\theta)$. Each of these points represents a 40-atom tripled spinel supercell with two vacant spinel cation positions. The gray band shows the range of measured volume differences.

minimizing mechanism, but rather are likely dependent on the preparation conditions. However, the results of Fig. 4 are independent of the *mechanism* of formation of $\gamma$ or $\eta$ (i.e., energetic, kinetic, or otherwise) and clearly show an indication of $O_h$ vacancies.

### V. SPINEL-BASED STRUCTURES: $HAl_5O_8$

We next turn to the issue of hydrogen in the spinel-based structures. The introduction of $H^+$ ions changes the stoichiometry, or the cation/anion ratio. Starting with $Al_2O_3$, electroneutrality requires the introduction of 3 $H^+$ ions with the removal of one $Al^{3+}$ ion. If we begin with our 40-atom $Al_{16}O_{24}$ cell, introduction of 3 H and removal of one Al result in $H_3Al_{15}O_{24}$, or $HAl_5O_8$. Thus, the stoichiometry can now be accommodated with only one spinel unit, $HAl_5O_8$ (14 atoms), and this ''hydrogen spinel'' has been suggested in the literature as a structural candidate for $\gamma$.[32,34] However, this primitive spinel cell will only have one ''vacancy'' (i.e., one spinel site in which Al is replaced by H), and so it is not possible to study ordering of Al and H with this primitive unit cell. Hence, we have also performed some calculations for supercells containing three spinel units (42 atoms), or three H atoms. All calculations described in this section and the next are performed within the GGA.

For the 14-atom primitive spinel cell, there are two choices: H in either a tetrahedral or octahedral position. We find that the two structures are nearly degenerate in energy, with the hydrogen in octahedral positions very slightly preferred. In both cells, H moves off a nominal, high-symmetry site to neighbor close to one of the surrounding oxygens (with H-O $\sim 1$ Å). However, for simplicity, we will refer to the hydrogen in these structures as being in ''octahedral'' or ''tetrahedral'' positions.[72]

For the tripled spinel unit cells, initially three cells were calculated: two cells with three octahedral hydrogen (one with the Al ''vacancies'' close together and one with them are far apart) and one with three tetrahedral hydrogen close together. The energetics of these three structures along with the two 14-atom primitive cells are shown in Fig. 5. Hydrogen in the spinel proves to be a ''great equalizer'': The strong energetic preference on vacancy configuration observed in the anhydrous case (Fig. 3) is greatly diminished, and now each of the cells is nearly degenerate: Despite the fact that the three 42-atom supercells have widely differing cation configurations, their calculated energies differ by only 0.005 eV/formula unit. This is an enormous contrast to the energies of the anhydrous cells which span a range of 0.33 eV/formula unit. For each of the three tripled supercells, the energy is below that of the 14-atom cells. This energy lowering is due to the fact that in the 14-atom cell, there is only one H atom, periodically repeated in each cell. Thus, each of the H atoms is in the same position as every other H atom. Lifting this constraint by tripling the unit cell and allowing the three H atoms to relax independently lowers the energy by a small amount.

The tripled supercells considered thus far contained three cation sites not occupied by an Al atom, with a single H nominally connected with each of the three sites. For each of the supercells, additional calculations were performed with different distributions of hydrogen. In addition to having one H in each of the three vacant sites (which we refer to as ''1+1+1''), we also considered having two H in one of the vacant sites and the third H in a different vacant site (''2+1+0''), and finally all three H in the same vacant site (''3+0+0''). The results of these calculations are shown in Fig. 6. The supercell with $T_d$ vacancies is more stable with the H ions distributed one per vacancy than with multiple H atoms per vacant site. However, the supercells with $O_h$ vacancies slightly prefer multiple H atoms per vacant site. The lowest energy state corresponds to the supercell with neighboring $O_h$ vacancies, and all three H atoms in a single vacant site. Thus, the combination of H in the spinel and multiple H per site serves to qualitatively reverse the strong cation/vacancy ordering tendency observed in the anhydrous calculations:

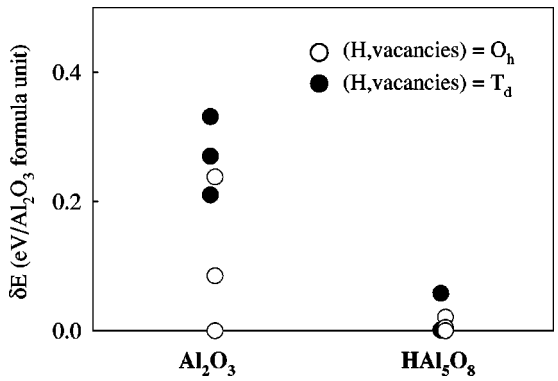


FIG. 5. The configuration dependence of the energetics of spinel-based $Al_2O_3$ and $HAl_5O_8$ cells (eV/$Al_2O_3$ formula unit, or eV/2 Al cations in the $HAl_5O_8$ calculations). Note the greatly diminished configuration dependence of the energy in the presence of hydrogen. The zeroes of energy in this figure are arbitrary (i.e., the zero of energy for the $Al_2O_3$ configurations has no relation to the zero of energy for the $HAl_5O_8$ configurations). For the $HAl_5O_8$ energies, the two higher energy points represent the 14-atom primative spinel cells with one H per cell, whereas the three lower energy points (nearly degenerate) represent the 42-atom tripled spinel cells with three H per cell.

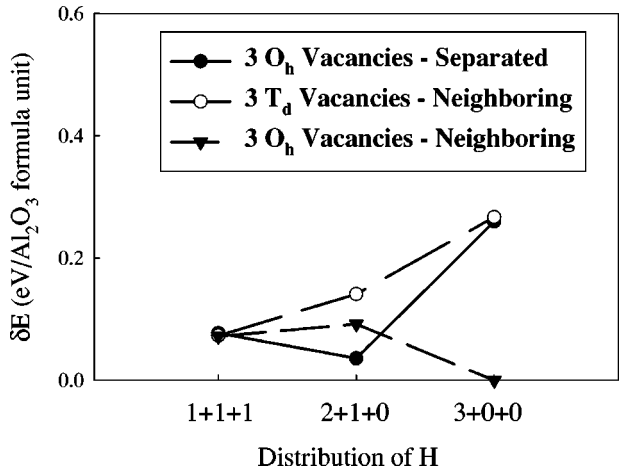


FIG. 6. Energetics (eV/2 Al cations) of tripled $HAl_5O_8$ supercells with multiple H per vacant site. The zero of energy in this figure is arbitrary.

TABLE VI. Comparison of calculated and experimental free energies of transformation $\Delta G_{298K}$ between corundum, boehmite, and gibbsite (kJ/mole). The calculated values of $\Delta G$ are given by a combination of first-principles $T=0$ K energetics (at zero pressure), plus the thermochemical data for $H_2O$ at $T=298$ K, as in Eq. (6). To demonstrate the importance of including the thermochemical data of $H_2O$ in these transformation free energies, calculated results are also shown without using Eq. (6)

| Reactant/Product | Reaction | Calculated | | Experimental |
|---|---|---|---|---|
| | | without Eq. (6) | with Eq. (6) | |
| corundum / boehmite | $Al_2O_3 + H_2O \rightarrow 2AlOOH$ | -86.4 | -21.6 | -25.9[a] |
| boehmite / gibbsite | $AlOOH + H_2O \rightarrow Al(OH)_3$ | -55.3 | +9.5 | $\sim -19$ to $+12$[b] |
| corundum / gibbsite | $\frac{1}{3}Al_2O_3 + H_2O \rightarrow \frac{2}{3}Al(OH)_3$ | -65.7 | -0.9 | -13.9[c] |

[a]Reference 74.
[b]Reference 75.
[c]Reference 74.

clustering of Al vacancies is weakly preferred in $HAl_5O_8$. It is interesting to note that here, just as in the anhydrous case, the clusters of vacancies show some form of instability: For the anhydrous defect spinels, near-neighboring vacancies showed an instability (either spontaneous or with an energetic barrier) towards Al cation motion into nonspinel sites. For the hydrogen spinels, neighboring vacancies show an instability towards the incorporation of multiple hydrogen per site.

### VI. PHASE STABILITY OF $Al_2O_3$, $HAl_5O_8$, AND AlOOH

We next turn to the relative phase stability of the spinel based-$Al_2O_3$ and $HAl_5O_8$ cells and boehmite, $\gamma$-AlOOH. Naturally, it is impossible to directly compare the energies of two compounds with different stoichiometries. However, since $Al_2O_3$ (and possibly $HAl_5O_8$) evolves from its precursor, AlOOH, by liberating $H_2O$, one can use the energy of $H_2O$ as a reference point for the comparison. In other words, one should compare the energy of $Al_2O_3 + nH_2O$ with $HAl_5O_8$ and AlOOH:

$$E(Al_2O_3) + \frac{1}{5}E(H_2O) \rightarrow \frac{2}{5}E(HAl_5O_8) \tag{2}$$

and

$$E(Al_2O_3) + E(H_2O) \rightarrow 2E(AlOOH). \tag{3}$$

Also, we note that the phase stability between the three compounds can be compared without reference to $H_2O$:

$$2E(Al_2O_3) + E(AlOOH) \rightarrow E(HAl_5O_8). \tag{4}$$

In the previous sections, we have described the energetic calculation of each of the terms in Eqs. (2)–(4) except that of $E(H_2O)$. To that end, we have performed a GGA calculation of an isolated $H_2O$ molecule in a cubic supercell (with periodic boundary conditions) with side lengths of 8, 10, and 12 Å . The energies of these three cells differed from one another by less than 0.002 eV/cell, so the result was taken as the energy of an isolated $H_2O$ molecule, $E^{GGA}_{H_2O}$, converged with respect to the supercell size. Using this calculated energy, we could compute the energies of each of the transformations in Eqs. (2)–(4). However, we really wish to compare the free energies of the reactions in these equations, for which the energy of a static, isolated $H_2O$ molecule at $T=0$ K is a very poor reference point since it is essentially the unphysical energy corresponding to the infinite temperature limit (isolated molecule) calculated with no entropic contributions. For a more reasonable comparison of the dehydration of boehmite into $Al_2O_3$, we must supplement the GGA-calculated energy of the isolated molecule with the entropic contributions of the liquid and gas phases of $H_2O$ and the enthalpy difference between these phases. For instance, we use the following expression for the (zero-pressure) Gibbs free energy of gas-phase $H_2O$:

$$G^{gas}_{H_2O} = E^{GGA}_{H_2O} - TS^{gas.}_{H_2O}. \tag{5}$$

For liquid phase, we use

$$G^{liq.}_{H_2O} = E^{GGA}_{H_2O} + \Delta H^{liq.-gas}_{H_2O} - TS^{liq.}_{H_2O}. \tag{6}$$

The entropic contributions $S^{gas}_{H_2O} = 188.83$ J/K mole, and $S^{liq.}_{H_2O} = 69.91$ J/K mole, and the enthalpy difference $\Delta H^{liq.-gas}_{H_2O} = -44.01$ kJ/mole have been tabulated in Ref. 73. In this discussion, we neglect the entropic contributions to the solid-state phases, $Al_2O_3$, AlOOH, and $HAl_5O_8$, which are presumably much smaller than the entropic contribution of $H_2O$.

Because this combination of first-principles energies with measured thermochemical data may seem a bit clumsy, we critically assessed its accuracy by comparing the calculated and measured free energies of the reactions between corundum, boehmite, and gibbsite:

$$Al_2O_3(\text{corundum}) + H_2O \rightarrow 2\,AlOOH(\text{boehmite}), \tag{7}$$

$$AlOOH(\text{boehmite}) + H_2O \rightarrow Al(OH)_3(\text{gibbsite}), \tag{8}$$

and

$$\frac{1}{3}Al_2O_3(\text{corundum}) + H_2O \rightarrow \frac{2}{3}Al(OH)_3(\text{gibbsite}). \tag{9}$$

The calculated and experimental results are given in Table VI. Using the VASP GGA energies for corundum, boehmite,

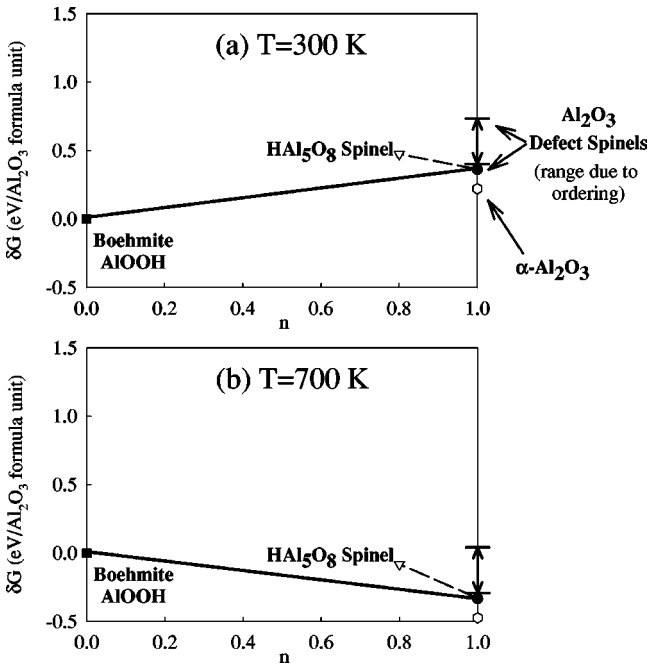


FIG. 7. Calculated phase stability between boehmite ($\gamma$-AlOOH), defect spinel-based ($\gamma, \delta, \eta$)-$Al_2O_3$, and the hydrogen spinel $HAl_5O_8$ at (a) $T=300$ K and (b) $T=700$ K. For the defect spinels, the full range of calculated energies (Fig. 3) is indicated, whereas for the hydrogen spinel $HAl_5O_8$ structure, only the lowest-energy state (see Fig. 6) is indicated.

gibbsite, and the $H_2O$ molecule, along with the thermochemical data for $H_2O$, we calculate transformation free energies in reasonable agreement with measured values.[74,75] Also shown in Table VI are the calculated results using only the energy of the isolated molecule $H_2O$ without reference to the thermochemical data of Eq. (6). In this case, one erroneously obtains unreasonably large values for the transformation free energies. Therefore, it is imperative to include the entropic and enthalpic corrections to the energy of an isolated $H_2O$ molecule in order to meaningfully compare the relative phase stabilities of the aluminum oxides with the aluminum hydroxides.

A similar combination of GGA energies and Eqs. (5) and (6) allows us to compare the phase stabilities of boehmite, $\gamma$-$Al_2O_3$, and the hydrogen spinel. Figure 7 shows the calculated phase stability at two temperatures, $T=300$ K and $T=700$ K. All the energies are given with respect to boehmite for stoichiometry $Al_2O_3+(1-n)H_2O$ in units of eV/$Al_2O_3$ formula unit. We note the following: (1) The hydrogen spinel is thermodynamically unstable with respect to decomposition into boehmite plus the anhydrous spinel-based $Al_2O_3$. Note that this conclusion follows directly from Eq. (4), and thus is independent of the energy of $H_2O$, and in our calculations is also independent of temperature. If we assume that the lowest-energy spinel-based structure is comparable to the energy of $\delta$, this means that $HAl_5O_8$ is thermodynamically unstable with respect to $\delta$-$Al_2O_3$ + boehmite. If we assume that $\gamma$-$Al_2O_3$ corresponds to a more disordered arrangement of $O_h$ vacancies (as Figs. 3 and 4 would suggest), then the energy of this disordered configuration is presumably somewhat closer to the middle of the range of the spinel supercells. Then, the hydrogen spinel is nearly degenerate in energy with boehmite + $\gamma$. This near degeneracy with hydrogen content could be responsible for some of the widely varying measurements of hydrogen contents in $\gamma$-aluminas. Also, the calculated thermodynamic instability (or, near degeneracy) does not, of course, preclude the possibility that the hydrogen spinel could form as a result of *kinetic* consequences. One should further note that this thermodynamic instability (or near degeneracy) of the hydrogen spinel is in qualitative contrast with the results of Sohlberg *et al.*,[34] who found an energetically strongly favored $HAl_5O_8$ spinel to be thermodynamically stable. (2) As the temperature is increased, the free energy of $H_2O$ decreases, and so the free energy of $Al_2O_3+H_2O$ drops relative to AlOOH. At room temperature the free energy of boehmite is below the defect spinel $Al_2O_3+H_2O$. However, at some temperature, $T_{tr}$, the entropic contribution to Eq. (5) will reverse this stability. For instance, in Fig. 7(b), one can see that at $T=700$ K the lowest energy spinels are already lower in energy than boehmite. Since there is a range of energies of the calculated defect spinels, there will be a range of temperatures for which the free energy of defect spinel $Al_2O_3+H_2O$ becomes lower than that of boehmite. From the energetics of Fig. 7, we calculate the range of temperatures to be $T_{tr}\sim 300-500\,^{\circ}$C. This temperature range is *precisely* the same as the observed temperature range required to dehydrate boehmite into $\gamma$-$Al_2O_3$ ($T_{tr}\sim 300-500\,^{\circ}$C).[2] This suggests that the final product of the transformation between boehmite and $\gamma$-$Al_2O_3$ may be strongly dependent on temperature: at low values of the transformation temperature (near 300 °C), only the relatively low-energy defect spinel states (with $O_h$ vacancies) are lower in energy than boehmite, whereas near 500 °C, the full range of spinel configurations are ''available'' for transformation. Of course, since the transformation of $\gamma$ into $\delta$ (a more ordered spinel-based structure) does not take place until 800–900 °C, there are obviously kinetic limitations to the available spinel configurations which are available for transformation at lower temperatures. Our work demonstrates that there are thermodynamic limitations as well in the range of $T_{tr}\sim 300-500\,^{\circ}$C.

## VII. POSSIBLE IMPLICATIONS FOR POROSITY

One of the key properties of the spinel-based transition aluminas which leads to their technological relevance is porosity. While transition aluminas prepared by either anodization of Al or plasma spraying of alumina powder can be fully dense,[1] dehydration of boehmite produces a high surface-area, highly porous microstructure of $\gamma$-$Al_2O_3$. In fact, McHale *et al.*[30] have demonstrated that as the surface area increases, the free energy of the $\gamma$ phase can actually drop below that of $\alpha$. Several dehydration mechanisms consistent with the formation of a porous microstructure have been suggested. From considerations of the crystallographic relationships between the boehmite and $\gamma$-$Al_2O_3$,[10] a mechanism has been proposed whereby internal $H_2O$ is elimated from the layered boehmite structure by condensation of protons and hydroxyl groups, followed by a collapse of the layered oxy-

gen network. While a porous microstructure would not necessarily result directly from this mechanism, the strains resulting from the collapse could cause the formation of cracks, and lead to pore formation. Alternatively, Ball and Taylor[76] suggested that the dehydration of brucite, $Mg(OH)_2$, involves mobile protons migrating from one region of the crystal (the ''acceptor'' region) to another region (the ''donor'' region), combining with hydroxyl groups in the donor region to form $H_2O$ (which subsequently leaves the crystal), and the countermigration of the Mg ion from the donor to the acceptor region, leaving behind a ''pore'' in the donor region, and MgO in the acceptor region. In this mechanism, the porous microstructure would be a necessary result of the reaction process. Wilson[20] has proposed a dehydration mechanism for boehmite somewhat intermediate between the ''collapse'' and brucite mechanisms: protons diffuse out of the layered boehmite structure between layers, and countermigrating Al ions fill the resulting spaces. A smaller version of the ''collapse'' mechanism then results in order for the oxygen sublattice to become fcc, and $H_2O$ is eliminated by the combination of protons with oxygen anions and hydroxyl groups in the ''donor'' region, forming pores. Wilson[20] has demonstrated that the observed lamellar (001) pore microstructure is consistent with this mechanism.

While we have not specifically addressed the *mechanism* of dehydration, our calculations of the relative phase stability of boehmite and $\gamma$-$Al_2O_3$ suggest several points about the *energetics* of the dehydration process: The fact that our thermodynamically calculated value of the boehmite/$\gamma$-$Al_2O_3$ transformation temperature is in agreement with the observed onset temperature for dehydration suggests that the initial stage of the dehydration could be driven by thermodynamic considerations. In other words the initiation of the transformation need not be driven by some kinetic mechanism of ionic diffusion which only becomes active at $T_{tr}$. Rather, it appears that the H may be mobile, and only when the free energy of $\gamma$-$Al_2O_3+H_2O$ becomes lower than that of $\gamma$-AlOOH does the transformation start. In fact, there is evidence for significant proton mobility in boehmite,[77–79] even at temperatures below the onset of dehydration. However, the fact that the $\gamma\rightarrow\delta$ and $\delta\rightarrow\theta$ (cation ordering of the spinel and fcc frameworks, respectively) transformations occur only at higher temperatures suggests that the motion of Al cations is at least partly kinetically limited (within $\gamma$-$Al_2O_3$, but not necessarily $\gamma$-AlOOH), and that these atoms cannot move freely until higher temperatures. If Al cations could freely move throughout both surface and bulk $\gamma$-$Al_2O_3$ at lower temperatures ($T\sim300-500\,^{\circ}C$), then our calculations suggest that the $\theta$ structure (the lowest-energy fcc-based alumina) should form at these lower temperatures. The final transformation in the dehydration sequence, $\theta\rightarrow\alpha$, does not occur until still higher temperatures. This final step to the equilibrium phase requires an fcc$\rightarrow$hcp rearrangement of the oxygen sublattice, suggesting that the oxygen anions are the most limited kinetically.

We also note that our calculations in Fig. 6 show that clusters of neighboring vacancies can lower their energy by incorporating multiple hydrogen atoms per site. This type of favored vacancy cluster could be an indication, albeit on an extremely small scale, of a hydrated pore, or ''nanopore.'' This vacancy clustering could also be a small-scale indication of the energetically favored boehmite + $\gamma$-$Al_2O_3$ phase-separation tendency, demonstrated in Fig. 7. In characterizing the lamellar pore structure of $\gamma$-$Al_2O_3$, Wilson[20] has noted the analogy with the eutectic lamellar microstructures found in metallurgical systems. The relevant transformation here is, with increasing temperature, from one solid phase (boehmite) to a two-phase mixture of a second solid phase ($\gamma$-$Al_2O_3$) and a ''liquid'' (or gas) phase ($H_2O$). If this transformation were a true, equilibrium thermodynamic transition, it would be analogous to a peritectic reaction rather than a eutectic reaction. Therefore, a comparison of generic peritectic microstructures with the pore structure of $\gamma$-$Al_2O_3$ could be of interest in elucidating the factors controlling porosity.

All the above statements concerning kinetic processes based on our thermodynamic calculations are of course extremely speculative. A more complete study of the diffusion of H and Al ions through boehmite and $\gamma$-$Al_2O_3$ (as well as $\delta$ and $\theta$) is clearly warranted. Such a study would not only yield a better understanding of the dehydration process, but it would likely provide new insights into the formation and control of porous microstructures in transition aluminas.

## VIII. CONCLUSIONS

Using first-principles total energy calculations, we have investigated the structure and phase stability of spinel-based transition aluminas ($\gamma$, $\delta$, $\eta$) in the presence and absence of hydrogen. We have critically assessed the accuracy of density functional based methods (VASP and FLAPW) using LDA and GGA exchange-correlation functionals for computing energetic and structural properties of transition aluminas and aluminum hydroxides, with both $O_h$ and $T_d$ coordinated Al cations. We have demonstrated the accuracy of structural quantities (lattice constants, cell volumes, bond lengths, etc.) and energetic quantities. The VASP-GGA calculations were shown to be highly accurate for oxides, oxyhydroxides, and hydroxides, and computationally efficient enough to allow the calculation of dozens of fully relaxed 40-atom cells (and several 80-atom cells).

For the anhydrous defect spinels, we find a strong energetic dependence on cation (Al/vacancy) configuration. Vacancies in octahedral sites are energetically preferred (or, Al cations prefer tetrahedral positions). This is consistent with the general preference of tetrahedral site occupation as one follows the sequence of Al cations in boehmite (100% $O_h$) through to $\theta$-$Al_2O_3$ (50% $O_h$). A comparison of the calculated cell volumes with density measurements also supports the preference of $O_h$ vacancies. There is a strong Al-vacancy ordering tendency, with widely separated vacancies being lower in energy than near-neighboring vacancies. However, closely spaced vacancies develop instabilities, often resulting in an energy lowering due to nonspinel site occupation. With near-neighboring $T_d$ and $O_h$ vacancies, a neighboring cation spontaneously falls from a spinel $T_d$ site ($8a$) into a nonspinel $O_h$ ($16c$) site. This is consistent with many observations of nonspinel occupation in $\gamma$, $\delta$, and $\eta$.

Upon incorporation of hydrogen into the structure, the strong cation-vacancy ordering tendency vanishes, and ''clusters'' of near-neighbor vacancies are slightly energetically preferred. Again, the clusters of vacancies show an instability in the sense that they can incorporate more than one hydrogen per vacant site. These hydrated vacancy clusters could represent a propensity of the material to form pores (or to phase separate). The hydrogen spinel ($HAl_5O_8$), proposed in the literature as a structural candidate for $\gamma$-alumina, is thermodynamically unstable with respect to decomposition into the anhydrous defect spinel plus boehmite ($\gamma$-AlOOH). Thus, we find no thermodynamic evidence for its formation, though we cannot rule out the possibility of its forming kinetically. By combining first-principles energetics with measured thermochemical data of $H_2O$, we have compared the phase stability of boehmite with the various phases of $Al_2O_3$ plus $H_2O$. We have computed the temperature range for which the free energies of the spinel-based aluminas (plus $H_2O$) becomes lower than that of boehmite. The temperature range is in excellent agreement with the observed transformation temperatures. This combination of first-principles energetics with thermochemical data for $H_2O$ yields transformation free energies of gibbsite, boehmite, and corundum in remarkably good agreement with measured data (often within the uncertainty of the measured data).

## ACKNOWLEDGMENTS

The authors gratefully acknowledge helpful discussions with many colleagues: Dr. A. Bogicevic, Dr. A. Drews, Dr. M. Finnis, Dr. C. Lowe-Ma, Dr. D. Nguyen-Manh, Dr. S. Pantelides, Dr. W. Schneider, Dr. K. Sohlberg, Dr. E. Stechel, Dr. F. Streitz, Dr. J. Sullivan, Dr. A. Sutton, Dr. D. Uy, Dr. W. Weber, and Dr. Y. Yourdshahyan.

[1] I. Levin and D. Brandon, J. Am. Ceram. Soc. **81**, 1995 (1998).
[2] K. Wefers and G. M. Bell, *Oxides and Hydroxides of Aluminum*, Alcoa Technical Paper No. 19 (Alcoa Laboratories, Pittsburgh, PA, 1987).
[3] W. H. Gitzen, *Alumina as a Ceramic Material* (Amer. Ceram. Soc., Columbus, OH, 1970).
[4] Some authors have noted (see Ref. 1) the absence of compelling experimental evidence for a direct $\delta \rightarrow \theta$ transformation, thus leaving open the possibility that both $\delta$ and $\theta$ could undergo a direct transformation to $\alpha$.
[5] C. L. Thomas, *Catalytic Processes and Proven Catalysts* (Academic, New York, 1970).
[6] B. C. Lippens and J. J. Steggerda, in *Physical and Chemical Aspects of Adsorbents and Catalysts*, edited by B. G. Linsen (Academic, New York, 1970), p. 171.
[7] H. Knözinger and P. Ratnasamy, Catal. Rev. Sci. Eng. **17**, 31 (1978).
[8] R. W. McCabe, R. K. Usmen, K. Ober, and H. S. Gandhi, J. Catal. **151**, 385 (1995).
[9] R.-S. Zhou and R. L. Snyder, Acta Crystallogr., Sect. B: Struct. Sci. **B47**, 617 (1991).
[10] B. C. Lippens and J. H. de Boer, Acta Crystallogr. **17**, 1312 (1964).
[11] S. J. Wilson, Proc. Br. Ceram. Soc. **28**, 281 (1979).
[12] H. Jagodzinski and H. Saalfeld, Z. Kristallogr. **110**, 197 (1958).
[13] K. P. Sinha and A. P. B. Sinha, J. Phys. Chem. **61**, 758 (1957).
[14] J. A. Wang, X. Bokhimi, A. Morales, O. Novaro, T. Lopez, and R. Gomez, J. Phys. Chem. B **103**, 299 (1999).
[15] K. Shirasuka, H. Yanagida, and G. Yamaguchi, Yogyo Kyokaishi **84**, 32 (1976).
[16] R. Dupree, M. H. Lewis, and M. E. Smith, Philos. Mag. A **53**, L17 (1986).
[17] Y. G. Wang, P. M. Bronsveld, J. Th. M. DeHosson, B. Djuricic, D. McGarry, and S. Pickering, J. Am. Ceram. Soc. **81**, 161 (1998).
[18] G. N. Kryukova, D. O. Klenov, A. S. Ivanova, and S. V. Tsybulya, J. Eur. Ceram. Soc. **20**, 1187 (2000).
[19] Y. Repelin and E. Husson, Mater. Res. Bull. **25**, 611 (1990).
[20] S. J. Wilson, J. Solid State Chem. **30**, 247 (1979).
[21] V. Jayaram and C. G. Levi, Acta Metall. **37**, 569 (1989).
[22] H. Saalfeld and B. B. Mehrotra, Ber. Dtsch. Keram. Ges. **42**, 161 (1965).
[23] E. J. W. Verwey, Z. Kristallogr. **91**, 317 (1935).
[24] C. S. John, N. C. M. Alma, and G. R. Hays, Appl. Catal. **6**, 341 (1983). These authors surprisingly suggest a $\theta$ phase with nearly exclusively octahedrally coordinated Al cations, in contrast to the commonly accepted $\beta$-$Ga_2O_3$-type structure in which 50% of the cations are $O_h$ and 50% are $T_d$.
[25] C. Pecharroman, I. Sobrados, J. E. Iglesias, T. Gonzalez-Carreno, and J. Sanz, J. Phys. Chem. B **103**, 6160 (1999).
[26] M.-H. Lee, C.-F. Cheng, V. Heine, and J. Klinowski, Chem. Phys. Lett. **265**, 673 (1997).
[27] V. A. Ushakov and E. M. Moroz, React. Kinet. Catal. Lett. **24**, 113 (1984).
[28] F. Ernst, P. Pirouz, and A. H. Heuer, Philos. Mag. A **63**, 259 (1991).
[29] S. Soled, J. Catal. **81**, 252 (1983).
[30] J. M. McHale, A. Auroux, A. J. Perrotta, and A. Navrotsky, Science **277**, 788 (1997).
[31] P. J. Eng, T. P. Trainor, G. E. Brown, Jr., G. A. Waychunas, M. Newville, S. R. Sutton, and M. L. Rivers, Science **288**, 1029 (2000).
[32] J. H. de Boer and G. M. M. Houben, *Proceedings of the International Symposium on the Reactivity of Solids* (Flanders Boktryckeri Aktieboolag, Göteburg, 1954), pp. 237–244.
[33] A. A. Tsyganenko, K. S. Smirnov, A. M. Rzhevskij, and P. P. Mardilovich, Mater. Chem. Phys. **26**, 35 (1990).
[34] K. Sohlberg, S. J. Pennycook, and S. T. Pantelides, J. Am. Chem. Soc. **121**, 7493 (1999).
[35] S.-D. Mo, Y.-N. Xu, and W.-Y. Ching, J. Am. Ceram. Soc. **80**, 1193 (1997).
[36] L. J. Alvarez, J. F. Sanz, M. J. Capitan, and J. A. Odriozola, Chem. Phys. Lett. **192**, 463 (1992).
[37] F. H. Streitz and J. W. Mintmire, Phys. Rev. B **60**, 773 (1999).
[38] M. Wilson, M. Exner, Y.-M. Huang, and M. W. Finnis, Phys. Rev. B **54**, 15 683 (1996).

[39] S. D. Kenny, D. Nguyen-Mahn, H. Fujitani, and A. P. Sutton, Philos. Mag. Lett. **78**, 469 (1998).
[40] A. Navrotsky, B. A. Wechsler, K. Geisinger, and F. Seifert, J. Am. Ceram. Soc. **69**, 418 (1986).
[41] M. R. Basila, Appl. Spectrosc. Rev. **1**, 289 (1968).
[42] M. L. Hair, *Infrared Spectroscopy in Surface Chemistry* (Dekker, New York, 1967), Chap. V.
[43] G. Yamaguchi, I. Yasui, and W.-C. Chiu, Bull. Chem. Soc. Jpn. **43**, 2487 (1970).
[44] L. M. Foster and H. C. Stumpf, J. Am. Chem. Soc. **73**, 1590 (1951).
[45] J. A. Kohn, G. Katz, and J. D. Broder, Am. Mineral. **42**, 398 (1957).
[46] R. Roy, V. G. Hill, and E. F. Osborn, Ind. Eng. Chem. **45**, 819 (1953).
[47] E. Husson and Y. Repelin, Eur. J. Solid State Inorg. Chem. **33**, 1223 (1996).
[48] K. E. Sickafus, J. M. Wills, and N. W. Grimes, J. Am. Ceram. Soc. **82**, 3279 (1999).
[49] The problem of $O_h$ vs $T_d$ site preference for cations in a spinel-based $\gamma$-$Al_2O_3$ is analogous to the normal/inverse spinel problem: ''Normal'' spinels, $A[B_2]O_4$, have $A$ cations in $T_d$ sites and $B$ cations in $O_h$ sites (denoted by brackets). However, there exists a class of ''inverse'' spinels, $B[AB]O_4$, in which $A$ cations are in $O_h$ sites, and the $B$ cations are split between $T_d$ and $O_h$ sites. The classification of normal and inverse spinels can be phrased in terms of $T_d$ vs $O_h$ cation site preference [see A. Navrotsky and O. J. Kleppa, J. Inorg. Nucl. Chem. **29**, 2701 (1967)].
[50] K. C. Hass, W. F. Schneider, A. Curioni, and W. Andreoni, Science **282**, 265 (1998).
[51] Y. Yourdshahyan, C. Ruberto, M. Halvarsson, L. Bengtsson, V. Langer, and B. I. Lundqvist, J. Am. Ceram. Soc. **82**, 1365 (1999); Y. Yourdshahyan, Ph.D. thesis, Chalmers University of Technology and Göteborg University, 1999; Y. Yourdshahyan and C. Ruberto (private communication).
[52] G. Kresse and J. Hafner, Phys. Rev. B **47**, 558 (1993); G. Kresse, thesis, Technische Universität Wien, 1993; G. Kresse and J. Furthmüller, Comput. Mater. Sci. **6**, 15 (1996); Phys. Rev. B **54**, 11 169 (1996).
[53] S.-H. Wei and H. Krakauer, Phys. Rev. Lett. **55**, 1200 (1985); D. J. Singh, *Planewaves, Pseudopotentials, and the LAPW Method* (Kluwer, Boston, 1994).
[54] D. M. Ceperley and B. J. Alder, Phys. Rev. Lett. **45**, 566 (1980).
[55] J. Perdew and A. Zunger, Phys. Rev. B **23**, 5048 (1981).
[56] D. Vanderbilt, Phys. Rev. B **41**, 7892 (1990).
[57] G. Kresse and J. Hafner, J. Phys.: Condens. Matter **6**, 8245 (1994).
[58] S. G. Louie, S. Froyen, and M. L. Cohen, Phys. Rev. B **26**, 1738 (1982).
[59] J. P. Perdew, in *Electronic Structure of Solids 1991*, edited by P. Ziesche and H. Eschrig (Akademie Verlag, Berlin, 1991), Vol. 11.
[60] J. C. Boettger, Phys. Rev. B **55**, 750 (1997).
[61] C. Corbato, R. T. Tettenhorst, and G. G. Christoph, Clays Clay Miner. **33**, 71 (1985).
[62] K. A. Wickersheim and G. K. Korpi, J. Chem. Phys. **42**, 579 (1965).
[63] F. Sim, S. St. Amant, I. Papai, and D. R. Salahub, J. Am. Chem. Soc. **114**, 4391 (1992).
[64] H. Saalfeld and M. Wedde, Z. Kristallogr. **139**, 129 (1974).
[65] T. Yokokawa and O. J. Kleppa, J. Phys. Chem. **68**, 3246 (1964).
[66] L. G. Ferreira, S.-H. Wei, and A. Zunger, Int. J. Supercomput. Appl. **5**, 34 (1991).
[67] S. Ansell, S. Krishnan, J. K. R. Weber, J. J. Felten, P. C. Nordine, M. A. Beno, D. L. Price, and M.-L. Saboungi, Phys. Rev. Lett. **78**, 464 (1997).
[68] D. R. Jennison, C. Verdozzi, P. A. Schultz, and M. P. Sears, Phys. Rev. B **59**, R15 605 (1999).
[69] We obtained point charges from the integrated charge density inside the muffin-tin spheres of the FLAPW calculations for $\theta$ (with the interstitial charge arbitrarily distributed in the ratio 1:3 to Al and O, respectively). This yields $q(\text{Al-}O_h) \sim +1.1$, $q(\text{Al-}T_d) \sim +1.2$, and $q(\text{O}) \sim 0.75$, in good agreement with charges obtained from previous first-principles calculations of $\alpha$- and $\theta$-$Al_2O_3$ [S.-D. Mo and W. Y. Ching, Phys. Rev. B **57**, 15 219 (1998).] With these charges, a simple point-charge Ewald calculation shows that tetrahedral sites have a more negative Coulomb potential and that vacancies prefer to separate themselves from one another. (Since simple point charges cannot be uniquely defined in terms of the more accurate three-dimensional charge density, several adjustments to the values of the point charges were made and the Ewald calculations repeated to verify the robustness of these conclusions.)
[70] One could construct a cluster expansion (a generalized Ising-like model) of the first-principles energetics in order to study the energetics of more complex vacancy configurations, such as random and partially ordered arrangements or to search for low-energy ground states [see, e.g., A. van der Ven and G. Ceder, Phys. Rev. B **59**, 742 (1999) for an example of a cluster expansion constructed for a spinel structure to study cation/vacancy ordering tendencies]. However, the spontaneous relaxation of cations into nonspinel sites complicates the construction of such a cluster expansion in that the configurational space of this problem cannot be constrained solely to a cation/vacancy ordering problem on the spinel lattice.
[71] In virtually every measured XRD pattern of $\gamma$, $\delta$, or $\theta$-$Al_2O_3$ in the literature, the largest peak in the profile occurs near $2\theta \sim 67°$. However, computed patterns for the defect-spinel cells (either with spinel-only or nonspinel occupation, both for $Al_2O_3$ and $HAl_5O_8$) of this work do not show the largest peak intensity at $2\theta \sim 67°$. We also computed the XRD pattern for $\theta$-$Al_2O_3$, ($\beta$-$Ga_2O_3$-type) using the positions of Zhou and Snyder (Ref. 9) obtained from neutron diffraction refinements. The calculated XRD pattern surprisingly does not yield the correct $2\theta \sim 67°$ peak. These transition aluminas are observed to have an abundance of defects present, which could cause significant changes in the diffraction patterns. The $\theta$ phase is reported to be highly twinned (Ref. 11) so much so that the monoclinic structure can appear to be orthorhombic. Also, given the high surface area of the transition aluminas, the fraction of surface atoms is relatively large, and can occupy ''nonspinel'' sites (Ref. 9). However, the ubiquitous nature of the 67° peak in virtually every measured XRD pattern of $\gamma$, $\delta$, and $\theta$, coupled with the absence of this peak in virtually every simulated pattern remains a mystery.
[72] In order to see the relaxation of H away from the high symmetry $T_d$ or $O_h$ sites, in the single spinel-unit $HAl_5O_8$ calculations, it

was necessary to artificially destroy all of the symmetry elements of the structure (e.g., by placing the H in a slightly displaced, low-symmetry position near the nominal tetrahedral or octahedral site), so these calculations were performed with $P1$ symmetry.

[73] P. W. Atkins, *Physical Chemistry*, 5th ed. (W. H. Freeman and Co., New York, 1994).

[74] P. Liu, T. Kendelewicz, G. E. Brown, Jr., E. J. Nelson, and S. A. Chambers, Surf. Sci. **417**, 53 (1998).

[75] P. H. Hsu, in *Minerals in Soil Environments* (Soil Science Society of America, Madison, WI, 1989), p. 331.

[76] M. C. Ball and H. F. W. Taylor, Miner. Mag. **32**, 754 (1961).

[77] J. J. Fripiat, H. Bosmans, and P. G. Rouxhet, J. Phys. Chem. **71**, 1097 (1967).

[78] A. Mata Arjona and J. J. Fripiat, Trans. Faraday Soc. **63**, 2936 (1967).

[79] J. J. Fripiat and R. Touillaux, Trans. Faraday Soc. **65**, 1236 (1969).

[80] W. E. Lee and K. P. D. Lagerlof, J. Electron Microsc. Tech. **2**, 247 (1985).

[81] L. Ouyang, Y.-N. Xu, and W. Y. Ching, Bull. Am. Phys. Soc. **44**, 1448 (1999).

[82] A. P. Borosy, B. Silvi, M. Allavena, and P. Nortier, J. Phys. Chem. **98**, 13 189 (1994).